# HUMIDITY VARIATIONS IN THE ATMOSPHERIC SURFACE LAYER

A Thesis

by

SCOTT RICHARD HUMPHREY

Submitted to the Graduate College of
Texas A&M University
in partial fulfillment of the requirement for the degree of

MASTER OF SCIENCE

May 1985

Major Subject: Meteorology

HUMIDITY VARIATIONS IN THE ATMOSPHERIC SURFACE LAYER

A Thesis

by

SCOTT RICHARD HUMPHREY

Approved as to style and content by:

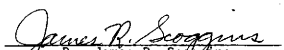

Dr. James R. Scoggins
(Chairman of Committee)

Dr. T. Steven Yuen
(Member)

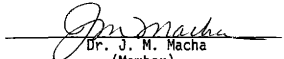

Dr. J. M. Macha
(Member)

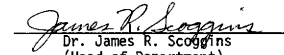

Dr. James R. Scoggins
(Head of Department)

May 1985

ABSTRACT

*Humidity Variations in the Atmospheric*
Surface Layer. (May 1985)
Scott Richard Humphrey, B.S., Texas A&M University
Chairman of Advisory Committee: Dr. James R. Scoggins

The turbulent fluctuations of humidity in the atmospheric surface layer are studied using field data consisting of high frequency wind velocity, temperature, and humidity measurements collected using a 22 m micrometeorological tower instrumented at three levels. These data are analyzed in the context of Monin-Obukhov similarity theory in order to confirm experimentally certain assumptions about the behavior of humidity variations.

This analysis includes the computation of humidity and sensible heat fluxes using eddy correlations, the computation of power spectra of both humidity and temperature fluctuations, an evaluation of the terms in the humidity variance budget equation, and the computation of humidity and temperature structure function parameters.

Comparisons are made between the behavior of humidity fluctuations and temperature fluctuations, and the results are also compared with those of previous investigators. It is found that humidity and temperature fluctuations behave similarly in the atmospheric surface layer, but there are some differences found between these results and those from previous studies.

ACKNOWLEDGMENT

I would like to express my sincere appreciation to Mr. Jake Canglose and Mr. Jerry Guynes, who set up and maintained the instrumentation for the field portion of this research. Without their dedication and professionalism this research would not have been possible.

I would also like to thank my committee chairman, Dr. James R. Scoggins, for his advice and guidance, and for making readily available to me all of the resources of the Department of Meteorology. In addition I would like to thank Dr. T. S. Yuen and Dr. J. M. Macha who also served on my graduate committee, the Aerospace Engineering Department for the use of their wind tunnel, and Mrs. Jacquelyn Strong for typing this manuscript.

TABLE OF CONTENTS

# LIST OF TABLES

# LIST OF FIGURES

List of Figures (Cont.)

List of Figures (Cont.)

# 1. INTRODUCTION

The purpose of this research is to study the turbulent fluctuations of humidity in the atmospheric surface layer. Humidity variations have not been widely studied in the past, and many of the assumptions about the nature of these variations have not been confirmed experimentally.

The specific objectives of this research are to:

1) establish the budget of humidity variance in the atmospheric surface layer, and to evaluate, using experimental data, the hypothesis that the humidity variance budget behaves like the temperature variance budget;
2) test the hypothesis that humidity and temperature flux-profile relationships have the same functional form;
3) relate the functional form of the humidity structure function parameter to that of the temperature structure function parameter;
4) test existing theory concerning the estimation of humidity flux using structure function parameters; and,
5) calibrate and test the reliability of the instrumentation and the data acquisition system used.

The experimental data used were gathered using the Texas A&M University Department of Meteorology's 22 m micrometeorological tower and associated instrumentation system, in a field experiment performed over an eight day period in May, 1984.

---

The style of this manuscript follows the format of the Journal of the Atmospheric Sciences.

## 2. THEORETICAL BACKGROUND

### a. General surface layer characteristics

The atmospheric surface layer is defined as the lowest portion of the planetary boundary layer where the fluxes of momentum, heat, and humidity can be considered constant with height. This surface layer or "constant flux layer" is found to vary in depth from about 20 m to 200 m (Lumley and Panofsky, 1964). Most early experimental studies of atmospheric turbulence focused on the surface layer because of the relative ease in gathering data.

Field studies using fast response wind and temperature sensors have been performed for more than 20 years, and researchers have developed many emperical relationships that describe the turbulent fluctuations of wind and temperature in the surface layer. These emperical relationships are necessary since turbulence in the surface layer has thus far defied theoretical description. However, not much attention has been paid by researchers to the variations of humidity in the surface layer. This is due mainly to the fact that until recently, dependable and inexpensive fast response humidity sensors have not been available. Since humidity and temperature are both scalar properties, it has been assumed that they follow the same emperical relationships. However, few attempts have been made to verify this assumption experimentally.

It has been found that the properties of wind velocity fluctuations in the surface layer can be nondimensionalized by a scaling parameter called the friction velocity, $u_*$, defined as

$$u_* = (\tau_o/\rho)^{1/2} \tag{2.1}$$

where $\tau_0$ is the frictional stress at Earth's surface and $\rho$ is the air density. Similarly, scaling parameters for temperature, $T_*$, and humidity, $q_*$, have also been defined and are given by

$$T_* = - Q_0/u_* \quad , \tag{2.2}$$

and

$$q_* = - M_0/u_* \tag{2.3}$$

where $Q_0$ is the surface heat flux, and $M_0$ is the surface moisture flux.

Most recent studies of turbulence in the surface layer are based on the similarity theory first put forth by Monin and Obukhov (1953, 1954). Through dimensional analysis, they reasoned that turbulence characteristics depend on five quantities: z, $\rho_0$, $g/T_0$, $u_*$, and $Q_0/C_p$, where z is the height above the ground, $\rho_0$ is the surface air density, g is the acceleration due to gravity, $T_0$ is the surface air temperature, and $C_p$ is the specific heat of air at constant pressure. When combined, these define a dimensionless stability parameter, z/L, where

$$L = \frac{u_*^3}{k \cdot g/T_0 \cdot Q/(C_p \rho_0)} \tag{2.4}$$

and k is von Karman's constant. The quantity L is called the Monin-Obukhov length, and it is a measure of the height above the ground above which the thermally generated turbulence dominates the mechanically generated turbulence (Lumley and Panofsky, 1964). Turbulence properties, when properly scaled, should show a functional dependence on the stability parameter, z/L.

The first extensive surface layer experiment was performed by the

Air Force Cambridge Research Laboratory in 1968 at a site in rural Kansas (Haugen et al., 1971). Analysis of the data collected confirmed the validity of Monin-Obukhov similarity theory, as well as determined the form of many of the emperical relationships that exist between turbulence properties and the stability parameter z/L. Subsequent studies using independent data sets also have given strong support to Monin-Obukhov theory, and it is in the context of this theory that most surface layer studies are now presented.

b. Spectra of turbulent fluctuations

When a harmonic analysis is made of a time series of the turbulent fluctuations of a property, the result is a spectrum of the turbulent fluctuations which shows the contributions of the different size oscillations to the total variance of that property. According to Kolmogorov's similarity theory, such spectra can be divided into three ranges, as shown in Fig. 1. In the dissipation range, where wavenumbers are high, molecular viscosity is the dominant factor in determining the shape of the spectrum, and in the low wavenumber range, large scale horizontal inhomogeneities are the dominant effect. However, in the inertial subrange, the shape of the spectrum is determined solely by dissipation, $\varepsilon$, which represents the rate at which energy is passed through this region to be dissipated by viscosity (Wyngaard, 1973).

By dimensional reasoning, the one dimensional spectrum for velocity fluctuations, for instance, should behave in the inertial subrange as

$$\phi_u(\kappa_1) = \alpha\varepsilon^{2/3}\kappa_1^{-5/3} \tag{2.5}$$

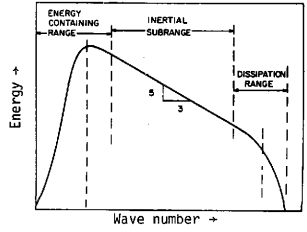


Fig. 1. Typical spectrum of turbulent fluctuations, showing the three ranges of turbulence (from Wyngaard, 1973).

where $\phi_u(\kappa_1)$ is the spectral density function for velocity fluctuations, $\varepsilon$ is the dissipation rate of turbulent kinetic energy, $\kappa_1$ is the longitudinal wavenumber, and $\alpha$ is a universal constant (Lumley and Panofsky, 1964). By dimensional reasoning and by analogy to velocity, the spectra for temperature and humidity in the inertial subrange should have the form

$$\phi_T(\kappa_1) = \beta_T \chi_T \varepsilon^{-1/3} \kappa_1^{-5/3} \tag{2.6}$$

and

$$\phi_q(\kappa_1) = \beta_q \chi_q \varepsilon^{-1/3} \kappa_1^{-5/3} \tag{2.7}$$

where $\phi_T(\kappa_1)$ and $\phi_q(\kappa_1)$ are the spectral density functions for temperature and humidity, respectively, $\chi_T$ and $\chi_q$ are the respective dissipation rates of the variance, and $\beta_T$ and $\beta_q$ are universal constants. Experimental results have confirmed the existence of the -5/3 power dependence on the wavenumber in the inertial subrange, and have determined

the values of the various universal constants (Panofsky, 1964; Kaimal et al., 1972).

c. Variance budgets

Using experimental data, researchers have calculated the budget of turbulent kinetic energy in the surface layer to determine the relationship that exists between production, dissipation, and turbulent transport of turbulent kinetic energy. In analogy to kinetic energy, budgets of the variances of scalar properties such as humidity can also be calculated. The equation that governs the budget of the variance of a property can be derived by taking the conservation equation for that property, breaking it into mean and perturbation components, and subjecting it to Reynold's averaging (Busch, 1973). Assuming horizontally homogeneous conditions, the equation takes the form

$$\frac{1}{2}\frac{\partial\overline{(s')}}{\partial t} = -\overline{s'w'}\frac{\partial\bar{s}}{\partial z} - D_s\overline{\frac{\partial s'}{\partial z}\frac{\partial s'}{\partial z}} - \frac{1}{2}\frac{\partial\overline{(w's's')}}{\partial z} \qquad (2.8)$$

where $\bar{s}$ and $s'$ are the mean and perturbation components of the scalar property, $D_s$ is the molecular diffusivity, and $w'$ is the perturbation vertical velocity. The first term is the time rate of change of the average variance, the second term is the production of the variance due to the interaction of the turbulent flux and the mean gradient, the third term is the rate of molecular dissipation of the variance, and the fourth term is the vertical flux divergence of the variance.

Wyngaard and Coté (1971) determined the budget of temperature variance, and found that production and molecular dissipation were in

local balance. The budget of humidity variance has been assumed to behave similarly, and Champagne et al. (1977) showed evidence that production and molecular dissipation of humidity variance are also in local balance. However, they did not directly measure most of the terms in the budget equation so their results are not totally conclusive.

d. Flux-profile relationships

The production terms in the energy budget and variance budget equations, when properly nondimensionalized, define dimensionless wind, temperature, and humidity profiles. These profiles take the form

$$\phi_m = \frac{kz}{u_*} \frac{\partial \bar{u}}{\partial z} \quad , \tag{2.9}$$

$$\phi_T = \frac{kz}{T_*} \frac{\partial \bar{T}}{\partial z} \quad , \tag{2.10}$$

and

$$\phi_q = \frac{kz}{q_*} \frac{\partial \bar{q}}{\partial z} \tag{2.11}$$

where $\phi_m$, $\phi_T$, and $\phi_q$ are the respective dimensionless profiles for velocity, temperature, and humidity, and all have a functional relationship with the stability parameter z/L. These relationships are called flux-profile relationships because when integrated, they yield expressions relating the flux with the mean profile of the given property. Various researchers have determined the forms of these relationships for velocity (momentum flux) and temperature from experiment (Businger et al., 1971; Webb, 1970; Dyer and Hicks, 1970), but the forms vary from one researcher to another and appear to depend on the instrument and

local topography (Yaglom, 1977). The humidity flux-profile relationship is thought to be identical to that of temperature, but few attempts have been made to verify this assumption experimentally.

e. Structure function parameters

One measure of the variability of a quantity is the structure function parameter defined as

$$D(r) = \overline{[f(x) - f(x+r)]^2} = C^2 r^{2/3} \tag{2.12}$$

where $r$ is the separation distance between two measurements, and $C^2$ is defined as the structure function parameter. In the inertial subrange for locally isotropic turbulence, the structure function parameter is related to the spectrum of the turbulent fluctuations by

$$\phi(\kappa) = 0.25C^2 \kappa^{-5/3} \tag{2.13}$$

where $\phi_\kappa$ is the spectral density function and $\kappa$ is the wavenumber (Wyngaard et al., 1971a). The temperature structure function parameter, $C_T^2$, has been calculated by Wyngaard et al. (1971a) and plotted against z/L. Later, Fairall et al. (1980) calculated the humidity structure function parameter, $C_q^2$, over the ocean and found it to vary with z/L by the same functional form, with the difference of only a constant.

## 3. INSTRUMENTATION AND DATA

### a. Specifications of instruments

The instrumentation system used for collecting turbulence data was assembled for the Texas A&M Department of Meteorology by the Climatronics Corporation. The system consists of three sets of fast response wind, temperature, and relative humidity sensors, as well as a data acquisition system and a tape drive to store the data on magnetic tape. These instruments were deployed at heights of 9.7 m, 15.2 m, and 20.9 m on a 22 m telescoping tower (Fig. 2). The physical separation of the instruments at any given tower level was less than one meter. All of the instruments were tested for response characteristics and were calibrated before being placed on the tower. A summary of the testing procedures and results will be presented here.

#### 1) Data acquisition system

The data acquisition system consists of wind component, temperature, and relative humidity translators which give continuous analog output from the sensors, and an IMP-803 rack-mounted microprocessor. The microprocessor polls each of the translators at intervals of 0.3 s, and converts the data from analog to digital form. The digital data is then sent to a Kennedy Model 9000 tape drive for storage on magnetic tape (Fig. 3). The wind component translator has a built-in filter with a time constant of 0.26 s, which helps to reduce electrical noise.

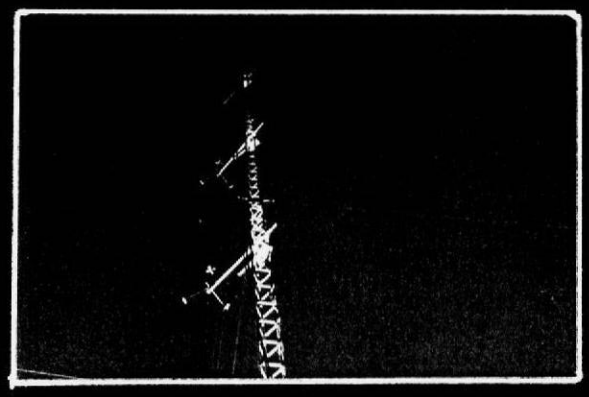

Fig. 2. Micrometeorological tower with instruments at 9.7 m, 15.2 m, and 20.9 m.

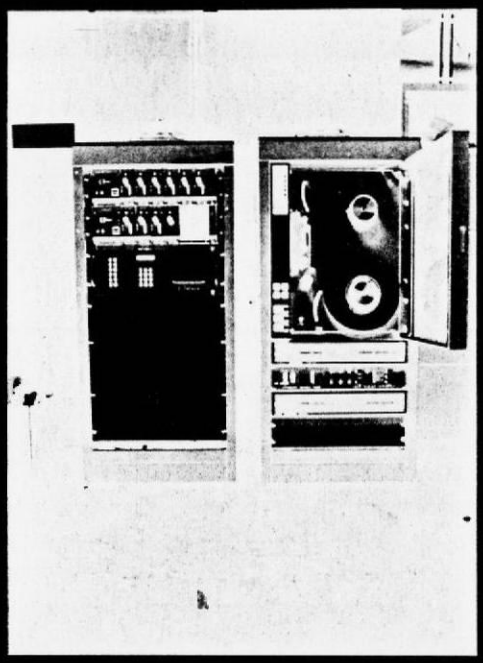

Fig. 3. Data acquisition system (left) and Kennedy Model 9000 tape drive (right).

2) Temperature sensors

The temperature sensors are Model 705 bead thermistors, mounted in a fan aspirated radiation shield (Fig. 4). The time constant of the sensor was measured between an ice bath and the ambient air, and the test output was taken from the stored digital data so as to include any bias introduced by the microprocessor or the temperature translator. The time constant was found to be 0.30 ± 0.02 s. All three temperature sensors were calibrated using an ice bath.

3) Humidity sensors

The humidity sensors are Vaisala Humicap Model HMP-14 humidity meters, placed in fan aspirated radiation shields (Fig. 5). The time constant was measured between two different chemical baths (LiCL solution, 2% relative humidity; $K_2SO_4$ solution, 100% relative humidity), and the ambient air. The time constant was found to be 0.40 ± 0.02 s. All sensors were then calibrated using the $K_2SO_4$ solution.

4) Wind sensors

The wind sensors are orthogonal arrays of u, v, w component sensors, comprised of WC-15 component transmitters fitted with Model 21282 polystyrene Gill helical propellors (Fig. 6). These "Gill type" anemometers were tested in a wind tunnel to determine their distance constants. The distance constant was found to be 1.10 ± 0.05 m. However, as mentioned earlier, the wind component translator has a built-in time constant of 0.26 s. Since the distance constant, L, is defined as

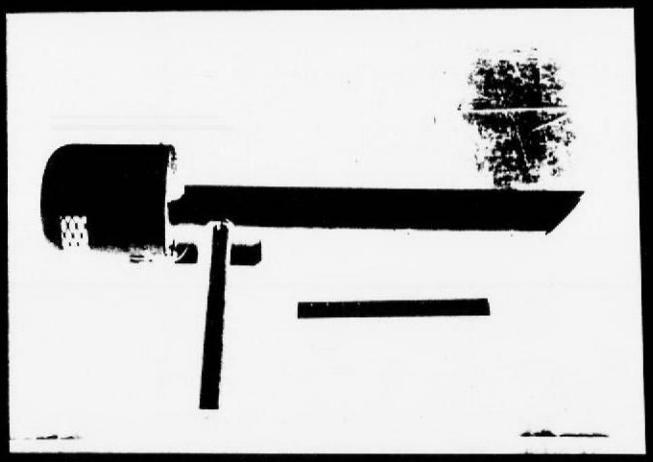

Fig. 4. Fan and radiation shields for the temperature and humidity sensors. The small tube protruding from the bottom of the fan houses the humidity sensor; the larger tube houses the temperature sensor.

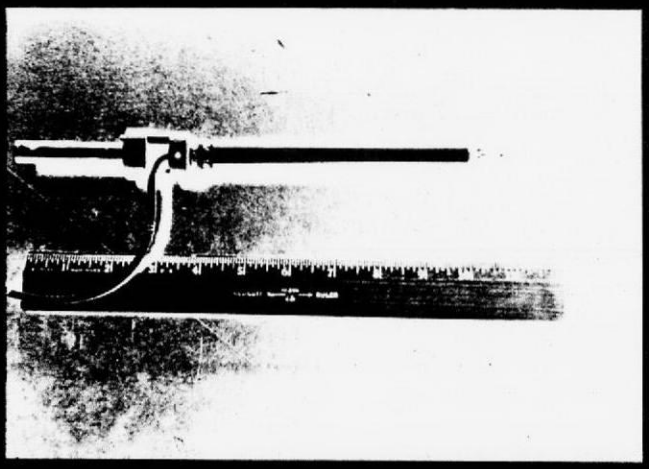

Fig. 5. The Vaisala Humicap humidity sensor. The sensing element is exposed on the right end of the sensor.

Fig. 6a. Orthogonal array of u, v, and w wind component sensors.

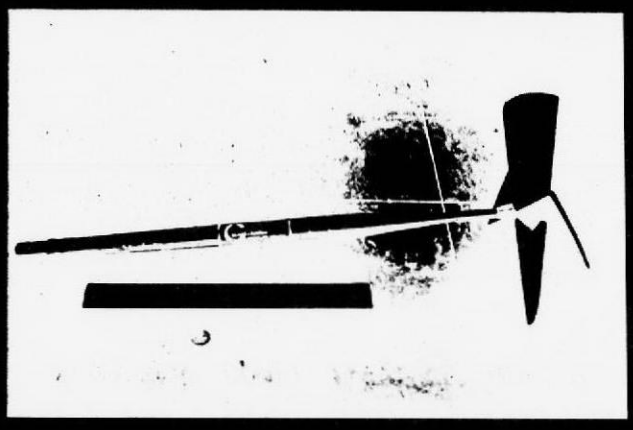

Fig. 6b. Closeup view of a single component anemometer.

$$L = U/T_t \tag{3.1}$$

where U is the wind speed and $T_t$ is the time constant, the effect of this filter is to increase the distance constant for increasing wind speeds. Table 1 summarizes the distance and time constants of the anemometers for several different wind speeds.

Table 1. Time constants and distance constants of anemometer for several wind speeds.

| Wind speed ($ms^{-1}$) | Time constant (s) | Distance constant (m) |
|---|---|---|
| 1.0 | 1.10 | 1.10 |
| 2.0 | 0.55 | 1.10 |
| 3.0 | 0.37 | 1.10 |
| 4.0 | 0.28 | 1.10 |
| 5.0 | 0.26 | 1.30 |
| 6.0 | 0.26 | 1.56 |
| 7.0 | 0.26 | 1.82 |
| 8.0 | 0.26 | 2.08 |

According to MacCready and Jex (1964), propellor anemometers are first order sensors, and their response to a sinusoidal input can be described by

$$M = (1 + \omega^2 T_t^2)^{-1/2} \tag{3.2}$$

where M is the amplitude ratio (as a function of frequency), $\omega$ is the circular frequency of oscillation of the input, and $T_t$ is the time constant. This anemometer response function was computed for five different wind speeds (Fig. 7). It can be seen that the response of the anemometers for a given frequency of oscillation is dependent on the

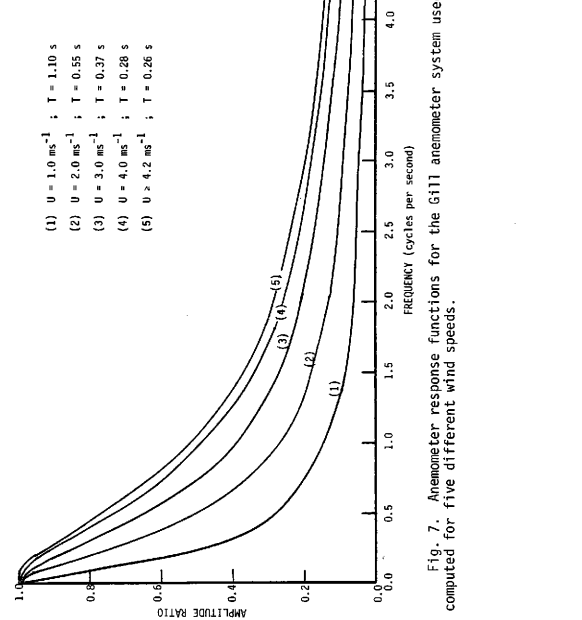


Fig. 7. Anemometer response functions for the Gill anemometer system used in this study, computed for five different wind speeds.

wind speed, with a larger amplitude ratio for higher wind speeds. In addition, for any given wind speed, the amplitude ratio decreases as you move toward higher input frequencies. However, it is important to note that since for all wind speeds greater than 4.2 $ms^{-1}$ the time constant is the same (Table 1), the frequency response function for all wind speeds greater than 4.2 $ms^{-1}$ is given by curve 5 in Fig. 6. Thus the frequency response of the instrument is not dependent on wind speed for high wind speeds. This characteristic results from the 0.26 s time constant inherent in the electronics.

5) Limitations imposed by instrument response

The slowest response time of all the instruments belongs to the relative humidity sensor, therefore it is this instrument that defines the resolution limitations imposed on the data. At a wind speed of 8 $ms^{-1}$, and with a time constant of 0.4 s (time constant of the humidity sensor), the smallest resolvable wavelength in the data is 6.4 m. At a wind speed of 3 $ms^{-1}$, the smallest resolvable wavelength decreases to 2.4 m. Most of the data in this study were collected with wind speeds in the range 3-8 $ms^{-1}$, therefore all wavelengths less than about 6 m will not be resolved in the data. The sampling rate, the physical separation of the instruments, and the filter in the wind component translator also impose wavelength restrictions, but these are smaller than that imposed by the humidity sensor.

Gill propellor anemometers should respond to an incident wind as the cosine of the angle that the wind makes with the propellor in order to correctly measure the component of the wind along the anemometer axis

(Drinkrow, 1972). Horst (1973) tested the response of Gill anemometers and found that the measured wind component differs slightly from the cosine response, with largest differences occurring for large angles of incidence. He found that the least amount of error is introduced when the u and v component sensors each make a 45° angle with the incident wind. In order to minimize this error, the u and v component sensors in this study were oriented towards roughly the northwest and the northeast, and the runs were chosen so that the prevailing wind was from the north as nearly as possible. No further adjustments were made to the wind data to correct for the differences from cosine response.

6) Other instrumentation used

Upper air soundings were made using an Airsonde and a TS-2AR portable receiving station, manufactured by Atmospheric Instrumentation Research, Inc. The airsonde measures pressure, temperature, and wet-bulb temperature, and sends the data to the receiving station where it is displayed in digital form. The data may be processed in real time using a modified HP-97 calculator, and the data are stored on magnetic tape using a standard cassette recorder.

b. Summary of data collected

1) Site and data collected

The tower was located on a rural site near the Brazos river bottom, approximately 15 km west of the Texas A&M campus. The surrounding land is used mostly for cattle grazing, and the vegetation was closely cropped at the time the data were collected. There were no major

topographical features or obstructions within 1000 m in the upwind direction (Fig. 8). The best exposure of the instruments on the tower was to the north, and winds blowing from between 260° and 090° (measured clockwise) were considered acceptable for gathering data.

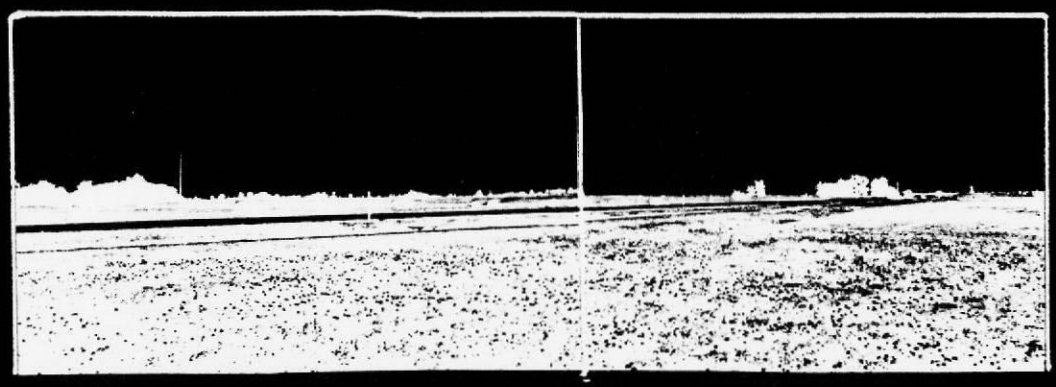

Fig. 8. View from micrometeorological tower towards the direction from which the wind was blowing for most of the runs selected. The left hand side is roughly 280° and the right hand side is roughly 040° (looking northward). The vertical line is the border between two photographs.

The turbulence data gathered consisted of 19 two-hour runs, taken over five different days. Most of the runs were made during a 3-day period when the winds were from the best direction considering the exposure of the instruments. Several upper air soundings were made throughout this 3-day period to determine the structure of the boundary layer and the lower atmosphere. Table 2 gives a summary of the different runs made and the surface conditions during each run.

2) Synoptic conditions

The area surrounding the tower site had endured several weeks of

Table 2. Summary of periods of turbulence data collected.

| Run # | Date | Time GMT | Temp deg F | RH % | Wind kts |
|---|---|---|---|---|---|
| 3 | 20 May | 1735-1935 | 80 | 72 | NE 10 |
| 4 | 23 May | 1935-2135 | 91 | 59 | NNE 4 |
| 5 | 28 May | 1615-1816 | 73 | 66 | NW 10 |
| 6 | 28 May | 1817-2018 | 79 | 53 | NW 12 |
| 7 | 28 May | 2019-2220 | 86 | 44 | NW 15 |
| 8 | 28 May | 2221-0022 | 85 | 44 | NNW 10 |
| 9 | 29 May | 0041-0242 | 81 | 56 | NNW 8 |
| 10 | 29 May | 0243-0443 | 76 | 53 | N 12 |
| 11 | 29 May | 1126-1327 | 56 | 68 | N 10 |
| 12 | 29 May | 1328-1529 | 59 | 61 | N 15 |
| 13 | 29 May | 1655-1856 | 70 | 43 | N 17 |
| 14 | 29 May | 1857-2058 | 74 | 36 | NE 20 |
| 15 | 29 May | 2100-2301 | 77 | 30 | NE 17 |
| 16 | 29 May | 2302-0103 | 76 | 29 | NNE 10 |
| 17 | 30 May | 0113-0314 | 71 | 34 | NNE 8 |
| 18 | 30 May | 0316-0517 | 63 | 47 | NE 5 |
| 19 | 30 May | 1030-1231 | 50 | 81 | NNE 5 |
| 20 | 30 May | 1232-1433 | 54 | 73 | NNE 7 |

dry weather prior to the period during which the data were collected. However, 11.4 cm of rain fell on the area between 18 May and 22 May, just prior to when the data were collected. This rain saturated the surface and provided a good source of moisture for evaporation. The 3-day period over which most of the data were collected (28 May through 30 May) followed the passage of a strong cold front on the morning of 28 May. This front brought cooler and drier air, and supplied strong northerly winds throughout the whole period. Fig. 9 shows a sounding made about 24 h after the passage of the cold front. The sounding shows a well mixed layer of dry air near the surface, capped by even drier air aloft. Skies were clear within a few hours of the passage of the front, and remained clear for the following three days. This lack of clouds

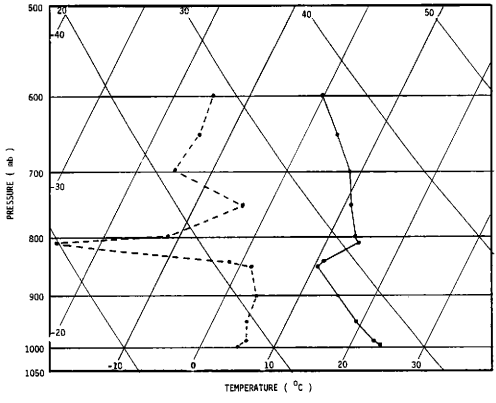


Fig. 9. Upper air sounding for 29 May, approximately 24 hours after the passage of a cold front. The solid line is temperature, and the dashed line is dewpoint temperature. Isotherms and adiabats are in degrees centigrade, pressure in millibars.

led to strong radiational cooling at night, and a resulting large diurnal temperature variations.

## 4. A THEORY OF HUMIDITY VARIANCE

As mentioned in Chapter 2, one can derive an equation governing the budget of humidity variance in the surface layer to determine the relationships that exist between production, dissipation, and turbulent transport of the variance. The usual form of this equation (2.8) includes simplifications with terms neglected in its derivation. Most investigators have not explored the possible contributions to the budget of humidity variance from these neglected terms. Therefore in this study, a rigorous derivation of the budget equation for humidity variance will be performed, and all terms that cannot be eliminated mathematically will be retained for further analysis.

To derive the budget equation, one begins with the conservation equation for humidity, given by

$$\frac{\partial q}{\partial t} + \frac{\partial u_j q}{\partial x_j} = D_q \frac{\partial^2 q}{\partial x_j^2} + Q_s \tag{4.1}$$

where $u_j$ is the three dimensional velocity tensor, $D_q$ is the molecular diffusivity of humidity, and $Q_s$ is a source and sink term. Next, separate the velocity, humidity, and source/sink term into mean and perturbation parts as follows:

$$q = \hat{q} + q' \quad ,$$

$$u_j = \hat{u}_j + u_j' \quad , \tag{4.2}$$

and $$Q_s = \hat{Q}_s + Q_s'$$

where the hatted terms are time dependent mean quantities. In this study, these mean parts of the quantities were defined using a weighted running average over a period of about 5 minutes. Substituting the values from (4.2) into (4.1) yields

$$\frac{\partial \hat{q}}{\partial t} + \frac{\partial q'}{\partial t} + \frac{\partial \hat{u}_j q'}{\partial x_j} + \frac{\partial u_j' \hat{q}}{\partial x_j} + \frac{\partial \hat{u}_j \hat{q}}{\partial x_j} + \frac{\partial u_j' q'}{\partial x_j} =$$

$$D_q \frac{\partial^2 \hat{q}}{\partial x_j^2} + D_q \frac{\partial^2 q'}{\partial x_j^2} + \hat{Q}_s + Q_s' \quad . \tag{4.3}$$

Next, to isolate the conservation equation for the mean part of the flow only, a long term average is taken of each of the terms in (4.3). In this study the averaging time used was 30 minutes, and these averages are denoted by an overbar. Note that in the averaging process, all averages of primed quantities alone cancel to zero by definition, but averages of terms that include products of mean and primed quantities such as $\overline{u_j' \hat{q}}$ do not become zero since the averaging time used in defining the time varying means is shorter than that denoted by the overbar. However, terms such as $\overline{\hat{u}_j q'}$ are zero. Thus the conservation equation for the mean part of the flow is

$$\frac{\partial \bar{q}}{\partial t} + \frac{\partial \overline{\hat{u}_j q'}}{\partial x_j} + \frac{\partial \overline{\hat{u}_j \hat{q}}}{\partial x_j} + \frac{\partial \overline{u_j' \hat{q}}}{\partial x_j} + \frac{\partial \overline{u_j' q'}}{\partial x_j} = D_q \frac{\partial^2 \bar{q}}{\partial x_j^2} + \overline{Q_s} \tag{4.4}$$

Subtracting (4.4) from (4.3) yields the conservation equation for the fluctuating part of the flow:

$$\frac{\partial q'}{\partial t} + \left[\frac{\partial \hat{q}}{\partial t} - \frac{\partial \bar{q}}{\partial t}\right] + \left[\frac{\partial \hat{u}_j q'}{\partial x_j} - \frac{\partial \overline{\hat{u}_j q'}}{\partial x_j}\right] + \left[\frac{\partial \hat{u}_j \hat{q}}{\partial x_j} - \frac{\partial \overline{\hat{u}_j \hat{q}}}{\partial x_j}\right] + \left[\frac{\partial u_j q'}{\partial x_j} - \frac{\partial \overline{u_j q'}}{\partial x_j}\right] +$$

$$\left[\frac{\partial u_j \hat{q}}{\partial x_j} - \frac{\partial \overline{u_j \hat{q}}}{\partial x_j}\right] = D_q \frac{\partial^2 q'}{\partial x_j^2} + \left[D_q \frac{\partial^2 \hat{q}}{\partial x_j^2} - D_q \frac{\partial^2 \bar{q}}{\partial x_j^2}\right] + Q_s' + \left[\hat{Q}_s - \bar{Q}_s\right] . \qquad (4.5)$$

Multiplying this equation by $q'$, and taking a 30 minute average yields the following budget equation for humidity variance:

$$\frac{1}{2}\frac{\partial \overline{(q')^2}}{\partial t} + \overline{q' \frac{\partial \hat{q}}{\partial t}} + \overline{q' \frac{\partial \hat{u}_j q'}{\partial x_j}} + \overline{q' \frac{\partial \hat{u}_j \hat{q}}{\partial x_j}} + \overline{q' \frac{\partial \hat{u}_j q'}{\partial x_j}} + \overline{q' \frac{\partial u_j \hat{q}}{\partial x_j}} =$$

$$- D_q \overline{\left(\frac{\partial q'}{\partial x_j}\right)^2} + D_q \overline{q' \frac{\partial^2 q'}{\partial x_j^2}} + \overline{q' Q_s'} + \overline{q' \hat{Q}_s} \quad . \qquad (4.6)$$

If one assumes isotropic turbulence, and breaks the divergence terms into their horizontal and vertical parts, this equation becomes

$$\frac{1}{2}\frac{\partial \overline{(q')^2}}{\partial t} + \overline{q'w'}\frac{\partial \hat{q}}{\partial z} + \frac{1}{2}\hat{w}\frac{\partial \overline{(q')^2}}{\partial z} + \frac{1}{2}\frac{\partial \overline{(q'q'w')}}{\partial z} + \varepsilon_q = \overline{q' Q_s'} + \left[\overline{q' \frac{\partial \hat{q}}{\partial t}}\right.$$

$$\left. - \overline{q' \frac{\partial \hat{u}_j \hat{q}}{\partial z}} + D_q \overline{q' \frac{\partial^2 \hat{q}}{\partial z}} + \overline{q' Q_s}\right] + \left[\overline{q'u'}\frac{\partial \hat{q}}{\partial x} + \overline{q'v'}\frac{\partial \hat{q}}{\partial y} + \frac{1}{2}\frac{\partial \overline{(q'q'u')}}{\partial x}\right.$$

$$\left. + \frac{1}{2}\frac{\partial \overline{(q'q'v')}}{\partial y} + \frac{1}{2}\hat{u}\frac{\partial \overline{(q')^2}}{\partial x} + \frac{1}{2}\hat{v}\frac{\partial \overline{(q')^2}}{\partial y}\right] \qquad (4.7)$$

where $$\varepsilon_q = - D_q \overline{\left(\frac{\partial q'}{\partial x_j}\right)^2} \quad . \tag{4.8}$$

The first bracket in (4.7) contains terms that result from the fact that the averaging time used in defining the mean quantities is shorter than that used in averaging the terms in the equation. The second bracket contains horizontal divergences and source/sink terms that cannot be computed using data from only one tower. Substituting R* for the first bracket, and R for the second bracket yields

$$\frac{1}{2}\overline{\frac{\partial (q')^2}{\partial t}} + \overline{q'w'}\frac{\partial \bar{q}}{\partial z} + \frac{1}{2}\overline{\frac{\partial (q'q'w')}{\partial z}} = - \varepsilon_q + R^* + R \quad . \tag{4.9}$$

If you use equal averaging times for defining the mean quantities and the overbar, this equation takes the classical form of the humidity variance budget equation

$$\frac{1}{2}\overline{\frac{\partial (q')^2}{\partial t}} + \overline{q'w'}\frac{\partial \bar{q}}{\partial z} + \frac{1}{2}\overline{\frac{\partial (q'q'w')}{\partial z}} = - \varepsilon_q + R \quad . \tag{4.10}$$

## 5. METHODS OF DATA ANALYSIS

### a. Data processing and filtering

Each of the 18 two-hour sets of turbulence data was processed to check for errors in the data. This processing included the computation of 5-min averages and standard deviations for each of the 15 channels of data as an initial check on the quality of the data. Some missing data were found (Table 3), which were primarily due to loose connections in the wind sensors. The fact that most of the v-component wind data at the middle tower level were lost did not affect the results since these winds were not needed for the final analysis. No obvious errors were found in the data, but some large step changes were found in the relative humidity data. By comparing the data at the different tower levels it was determined that these step changes were real and were not due to instrument error. The wind component data at all levels were adjusted to a north-south coordinate system, so that the data could be used in other studies with little confusion. After all the data were checked and winds translated, they were archived on magnetic tape for future use.

To put the data into a suitable form for the study of turbulence, the winds were translated into downwind and crosswind components, based on a one hour average wind direction. In addition, the relative humidity data were converted into specific humidity, q, in units of g(Kg). Next, the data were filtered so as to remove trends and long period fluctuations from the perturbation quantities. To achieve this, each 2-hr set of data was separated into two 1-hr parts, and subjected to an

Table 3. Summary of missing data.

| Run # | Missing data |
|---|---|
| 3 | v-component, middle level |
| 4 | v-component, middle level |
| 5 | v-component, middle level |
| 6 | v-component, middle level; u-component, upper level |
| 7 | v-component, middle level; u-component, upper level |
| 8 | v-component, middle level |
| 9 | v-component, middle level |
| 10 | v-component, middle level |
| 11 | None missing |
| 12 | None missing |
| 13 | v-component, middle level |
| 14 | v-component, middle level |
| 15 | v-component, middle level |
| 16 | v-component, middle level |
| 17 | v-component, middle level |
| 18 | v-component, middle level |
| 19 | v-component, middle level |
| 20 | v-component, middle level |

81 weight symmetrical low pass filter, with filter weights applied at every tenth data point outward from the central point. The filter weights used are listed in Table 4 and the frequency response function of the filter is shown in Fig. 10. Use of this low pass filter shortened each of the 1 hr data sets by 4 minutes because points outward from the central weight were dropped.

After the data were filtered, the resulting smoothed time series defined the mean (hatted) part of the original series, and the difference between the smoothed series and the original series defined the perturbation (primed) quantities (see Eqn. 4.2). For the most part, the primed quantities defined in this fashion include the fluctuations with periods of approximately 4 min or less. Finally, all primed and hatted quantities were stored on tape for later computations.

Table 4. Filter weights, $W_k$, for the running mean filter.

| K | $W_k$ | K | $W_k$ |
|---|---|---|---|
| 0 | .03002 | 21 | .00872 |
| 1 | .02985 | 22 | .00769 |
| 2 | .02968 | 23 | .00682 |
| 3 | .02881 | 24 | .00594 |
| 4 | .02870 | 25 | .00521 |
| 5 | .02791 | 26 | .00448 |
| 6 | .02713 | 27 | .00389 |
| 7 | .02610 | 28 | .00331 |
| 8 | .02507 | 29 | .00285 |
| 9 | .02386 | 30 | .00239 |
| 10 | .02266 | 31 | .00204 |
| 11 | .02134 | 32 | .00168 |
| 12 | .02002 | 33 | .00142 |
| 13 | .01866 | 34 | .00116 |
| 14 | .01730 | 35 | .00097 |
| 15 | .01595 | 36 | .00078 |
| 16 | .01461 | 37 | .00065 |
| 17 | .01334 | 38 | .00052 |
| 18 | .01207 | 39 | .00042 |
| 19 | .01091 | 40 | .00034 |
| 20 | .00974 | | |

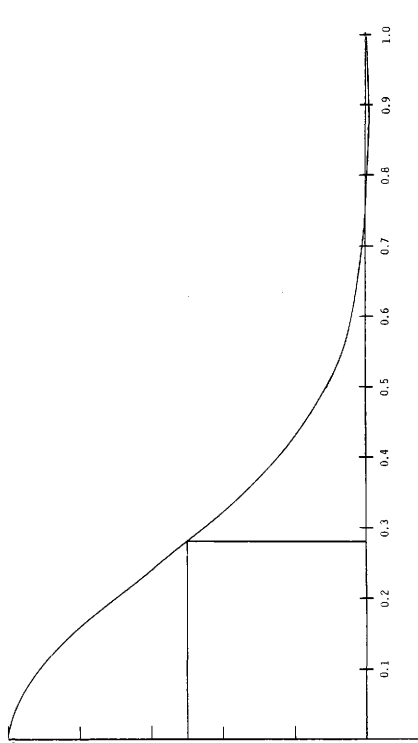


Fig. 10. Frequency response function of the filter used to separate mean and perturbation components of the measured variables. The vertical line indicates the value of the cutoff frequency corresponding to 50% amplitude ratio.

b. Computation of turbulence quantities

1) Fluxes and structure function parameters

Fluxes of momentum, heat, and moisture were computed for each data set using the eddy correlation technique. This technique uses the following approximations for the fluxes:

$$\tau = -\rho_o \overline{u'w'} \quad ,$$

$$H = C_p \rho_o \overline{T'w'} \quad ,$$

and

$$E = \rho_o \overline{q'w'} \qquad (5.1)$$

where $\tau$, H, and E are the momentum flux (or Reynold's stress), heat flux, and humidity flux, respectively, $\rho_o$ is the surface air density, and $C_p$ is the specific heat of air at constant pressure (Busch, 1973). In this study, only the covariances in these expressions were computed, not the fluxes themselves. The averaging time used in computing these covariances was 30 min.

The turbulence scaling parameters were also computed for 30-min periods using the above covariances by the relationships

$$u_* = (-\overline{w'u'})^{1/2},$$

$$T_* = -(\overline{T'w'})/u_* \quad ,$$

and

$$q_* = \overline{(q'w')}/u_* \quad . \tag{5.2}$$

In addition the stability parameter z/L was computed for 30-min periods at each tower level where

$$L = \frac{u_*^3 T_o}{Kg \overline{w'T'}} \quad , \tag{5.3}$$

and K and g are the Von Korman constant and gravity respectively.

2) Spectra and structure function parameters

Turbulence spectra were computed over 30-min periods for each of the data sets using the autocorrelation method (Panofsky and Brier, 1958). This method requires the computation of the autocorrelation function of the time series for m lags. The equation is

$$r_L = \frac{\sum (x_i)(x_{i+L})}{S_x^2 N} \tag{5.4}$$

where $r_L$ is the autocorrelation for lag L, $x_i$ and $x_{i+L}$ are the primed quantities at data points i and i+L respectively, $S_x^2$ is the variance for the 30-min period, and N is the total number of data points in the series. The spectral estimates are then computed using

$$B_i = \frac{r_o}{m} + \frac{2}{m} \sum_{L=1}^{m-1} \left[ r_L \cos \left( \frac{360°}{2m} + iL \right) \right] + \frac{r_m}{m} (-1)^i \tag{5.5}$$

where m is the maximum number of lags, and $B_i$ are the normalized

spectral estimates. If $B_i$ is plotted as a function of $i/2m\Delta t$, the result is the smoothed version of the normalized spectrum of the time series. Blackman and Tukey (1958) suggest that further smoothing of the spectrum using

$$S_i = .25\ B_{i-1} + .50\ B_i + .25\ B_{i+1} \tag{5.6}$$

will yield a better estimate of the spectrum. The more lags one uses in computing the autocorrelation function, the better the resolution of the spectrum becomes. However, using more lags adds considerably to the amount of computer time needed to compute the spectrum, so in this study only 200 lags were used since details of the spectrum were not needed for the analysis.

The most direct method of computing a structure function parameter uses (2.12) with measurements taken at a separation distance, r, where r is very small. In this study, the three tower levels where the measurements were made were too far apart to compute the structure function parameters using this method, so an alternate method was used. This alternate method uses the relationship between the structure function parameter and the spectrum of turbulent fluctuations shown in (2.13) to compute the different structure function parameters for wind, temperature and humidity. After Fairall et al. (1980), (2.13) can be put in the following form to compute the structure function parameters

$$C_x^2 = \frac{8}{3}\left(\frac{2\pi}{U}\right)^{2/3} \frac{(x^2)_{\ell,u}}{n_\ell^{-2/3} - n_u^{-2/3}} \tag{5.7}$$

where $n_\ell$ and $n_u$ are the lower and upper frequency limits of the spectrum

where the equation is applied, $(x^2)_{\ell,u}$ is the fraction of the total variance of the particular variable that is contained within these frequency limits, and U is the mean wind speed. The frequency limits should lie within the inertial subrange of the spectrum of the turbulent fluctuations for (5.7) to hold, and these limits were properly chosen to comply with this limitation.

3) Evaluation of the terms in the variance budget equation

It was possible to compute most of the terms in the humidity variance budget equation, given the data collected. This includes all of the terms in (4.9) and (4.10) except for the term R, which contains the horizontal divergences and source/sink terms. All of the barred terms in (4.9) and (4.10) were computed using 30-min averaging times, and those terms including vertical gradients were computed assuming a linear gradient between the top and bottom tower levels. The perturbation (primed) quantities had to be slightly adjusted so that they would sum to zero when averaged over 30 min, in accordance with the constraints of Reynold's averaging theory. The adjustment was small and apparently resulted from eliminating points during the filtering process.

The dissipation term, $\varepsilon_q$, was computed indirectly using the humidity and velocity structure function parameters, which themselves were computed from the spectra. The relationship used was

$$\varepsilon_q = \chi_q \frac{kz}{u_* q_*^2} , \tag{5.8}$$

where $\chi_q$ is the dimensionless dissipation rate, defined by

$$\chi_q = 0.125\ C_q^2\ (C_v^2)^{1/2}\ \alpha^{-1/2}\ \beta_q^{-1} \tag{5.9}$$

and $\alpha$ and $\beta_q$ are the spectral constants for velocity and humidity spectra, respectively (Wyngaard and Clifford, 1978). Values used for the constants were $\alpha = 0.5$, $\beta_q = 0.40$, and $k = 0.35$.

# 6. RESULTS

## a. General turbulence characteristics

Table 5 lists the computed turbulence scaling parameters for 30-min periods during each of the 18 runs. Runs 3 and 4 were made on two separate afternoons, while runs 5-20 were made nearly consecutively over a 3-day period following the passage of the cold front. No data were collected between 0100 and 0600 local time due to light winds.

Examination of the computed values of the stability parameter z/L shows that most values fell within the range -1.6 to 0.3, with the greatest number occurring on the slightly unstable side of neutral stability. If one follows the variation of z/L over one day (runs 10-18 for instance), one can see that positive values are found in the early morning and late evening, and negative values during the daylight hours as expected since z/L is directly proportional to the vertical heat flux.

The variation and range of the turbulence scaling parameters $u_*$, $T_*$, and $q_*$ can also be seen in Table 5. Since these quantities are directly proportional to the momentum, heat, and moisture fluxes in the vertical direction, they give an indication of the change in the direction and magnitudes of the fluxes over the time period. $u_*$ values are mostly in the range 0.2-0.4 $ms^{-1}$, with lower values occurring at night when the atmosphere was more stable. Any run with a value of $u_*$ less than 0.1 $ms^{-1}$ was not used in any of the analysis, since under such stable conditions the atmosphere becomes stratified and the turbulence properties between layers become decoupled. The negative $u_*$ values for

Table 5. Computed values of turbulence scaling parameters.

| Run # | z/L | $u_*$ $ms^{-1}$ | $T_*$ deg C | $q_*$ g $kg^{-1}$ |
|---|---|---|---|---|
| | | 20 May | | |
| 3A | -0.257 | 0.2112 | -0.0580 | -0.3186 |
| 3B | -1.553 | 0.1200 | -0.1131 | -0.7336 |
| 3C | -0.299 | 0.2001 | -0.0606 | -0.4601 |
| 3D | -0.356 | 0.2172 | -0.0851 | -0.4308 |
| | | 23 May | | |
| 4A | -4.911 | 0.0845 | -0.1796 | -0.8699 |
| 4B | -2.769 | 0.1066 | -0.1611 | -0.7006 |
| 4C | -2.522 | 0.1105 | -0.1580 | -0.8334 |
| 4D | -7.109 | 0.0336 | -0.4124 | -2.082 |
| | | 28 May | | |
| 5A | -0.017 | 0.3013 | -0.0079 | -0.0890 |
| 5B | -0.018 | 0.2893 | -0.0089 | -0.1109 |
| 5C | -0.020 | 0.3466 | -0.0122 | -0.1119 |
| 5D | -0.039 | 0.2834 | -0.0159 | -0.1286 |
| 6A | -0.065 | 0.2551 | -0.0215 | -0.1429 |
| 6B | -0.262 | 0.2635 | -0.0925 | -0.3936 |
| 6C | -0.191 | 0.2870 | -0.0800 | -0.3087 |
| 6D | -0.369 | 0.2284 | -0.0982 | -0.3620 |
| 7A | -0.219 | 0.2422 | -0.0655 | -0.2580 |
| 7B | -0.126 | 0.2418 | -0.0376 | -0.1818 |
| 7C | -0.083 | 0.2838 | -0.0341 | -0.1600 |
| 7C | -0.096 | 0.2284 | -0.0316 | -0.1311 |
| 8A | -0.024 | 0.2225 | -0.0060 | -0.0843 |
| 8B | -0.026 | 0.2583 | -0.0089 | -0.0775 |
| 8C | 0.001 | 0.3088 | -0.0184 | -0.0873 |
| 8D | 0.001 | 0.3543 | 0.0002 | -0.0465 |
| 9A | 0.017 | 0.2159 | 0.0041 | -0.0236 |
| 9B | 0.012 | 0.2592 | 0.0040 | -0.0194 |
| 9C | 0.010 | 0.3348 | 0.0055 | -0.0129 |
| 9D | 0.005 | 0.3280 | 0.0029 | -0.0296 |
| 10A | 0.015 | 0.3056 | 0.0072 | -0.0185 |
| 10B | 0.011 | 0.2913 | 0.0047 | -0.0248 |
| 10C | 0.010 | 0.3021 | 0.0044 | -0.0443 |
| 10D | 0.013 | 0.3134 | 0.0063 | -0.0464 |

Table 5. Continued.

| Run # | z/L | $u_*$ $ms^{-1}$ | $T_*$ deg C | $q_*$ $g\ kg^{-1}$ |
|---|---|---|---|---|
| | | 29 May | | |
| 11A | 0.004 | 0.3209 | -0.0019 | -0.0185 |
| 11B | -0.002 | 0.2585 | -0.0008 | -0.0248 |
| 11C | -0.030 | 0.2536 | -0.0096 | -0.0443 |
| 11D | -0.019 | 0.3622 | -0.0119 | -0.0464 |
| 12A | -0.033 | 0.4267 | -0.0298 | -0.0518 |
| 12B | -0.061 | 0.3445 | -0.0354 | -0.0532 |
| 12C | -0.094 | 0.3467 | -0.0554 | -0.0825 |
| 12D | -0.176 | 0.2740 | -0.0651 | -0.0878 |
| 13A | -0.274 | 0.2790 | -0.1058 | -0.1460 |
| 13B | -0.116 | 0.3541 | -0.0722 | -0.1451 |
| 13C | -0.215 | 0.2999 | -0.0964 | -0.1563 |
| 13D | -0.152 | 0.3438 | -0.0894 | -0.1503 |
| 14A | -0.219 | 0.2652 | -0.0769 | -0.1199 |
| 14B | -1.012 | 0.1621 | -0.1329 | -0.2646 |
| 14C | -0.144 | 0.3250 | -0.0759 | -0.1303 |
| 14D | -0.208 | 0.2619 | -0.0714 | -0.1457 |
| 15A | -0.223 | 0.2793 | -0.0874 | -0.0972 |
| 15B | -0.206 | 0.2753 | -0.0782 | -0.1194 |
| 15C | -0.085 | 0.3345 | -0.0477 | -0.1021 |
| 15D | -0.071 | 0.3241 | -0.0376 | -0.0771 |
| 16A | -0.073 | 0.2491 | -0.0228 | -0.0614 |
| 16B | -0.036 | 0.2640 | -0.0125 | -0.0508 |
| 16C | -0.013 | 0.2744 | -0.0049 | -0.0377 |
| 16D | 0.006 | 0.2046 | 0.0012 | -0.0320 |
| 17A | 0.077 | 0.1767 | 0.0120 | -0.0218 |
| 17B | 0.076 | 0.1532 | 0.0089 | -0.0219 |
| 17C | 0.113 | 0.1536 | 0.0132 | -0.0173 |
| 17D | 0.111 | 0.1192 | 0.0077 | -0.0163 |
| | | 29 May | | |
| 18A | 0.184 | 0.0963 | 0.0084 | -0.0194 |
| 18B | 0.132 | 0.0735 | 0.0034 | -0.0182 |
| 18C | 0.259 | 0.0515 | 0.0034 | -0.0146 |
| 18D | 0.787 | 0.0801 | 0.0090 | -0.0267 |

Table 5. Continued.

| Run # | z/L | $u_*$ $ms^{-1}$ | $T_*$ deg C | $q_*$ g $kg^{-1}$ |
|---|---|---|---|---|
| | | 30 May | | |
| 19A | -2.172 | -0.1612 | -0.0027 | -0.0081 |
| 19B | -3.145 | -0.2245 | -0.0077 | -0.0023 |
| 19C | 2.605 | -0.2520 | 0.0080 | -0.0042 |
| 19D | -0.520 | 0.2973 | -0.0022 | -0.0447 |
| 20A | -0.269 | -0.0934 | -0.0115 | -0.0788 |
| 20B | -0.143 | 0.1638 | -0.0188 | -0.1011 |
| 20C | -0.158 | 0.1629 | -0.0207 | -0.1224 |
| 30D | -0.106 | 0.1957 | -0.0201 | -0.1364 |

runs 19A-19C and 20A indicate that the momentum flux was away from the ground, which was up the mean wind gradient at this time. Although this is an unusual and significant situation which merits attention, it is beyond the scope of this study and will not be examined further at this time. Data from runs 19A-19D and 20A were not included in any of the analysis of the results for this reason. Negative values of $q_*$ were found for all of the runs, which indicated that the moisture flux was away from the ground, with smallest values occurring at night when the surface layer was stable. This result is not unusual since the ground was saturated and the air above it was quite dry throughout the whole period. A value for the roughness height, $z_o$, was calculated for each run with values ranging from 0.1-2.7 cm, depending on stability. This range of values agrees well with the observed roughness of the surrounding area, which was mostly closely cropped grass with some bare spots.

Fig. 11 is a plot of the normalized standard deviations of the humidity fluctuations against stability. According to Monin-Obukhov theory, if one assumes a condition of local free convection, these values should vary with stability as

$$- \sigma_q/q_* = b(-z/L)^{-1/3} \tag{6.1}$$

where b is an experimental constant (Wyngaard, 1973). A log-log plot against stability (Fig. 12) clearly shows this -1/3 power dependence. If you assume the -1/3 power relationship to apply to these data, a value of b = 0.5 can be estimated, which is in good agreement with a value of b = 0.48 calculated by Smedman-Högström (1973). Normalized standard deviations of temperature fluctuations should also follow (6.1), and plots of these values against stability appear in Figs. 13 and 14. Once again the -1/3 power dependence on stability is indicated, and a value of b = 1.1 is estimated for temperature. This is much higher than the value of b = 0.38 found by Smedman-Högström and by other investigators (Wyngaard et al., 1971b). These results bear out the assumption that the standard deviations of humidity and temperature fluctuations behave similarly. They both exhibit the same functional relationship with stability, with the difference of only a constant. However, this assumption should not be extended outside of the range of stabilities studied here.

One more significant characteristic of the general turbulence structure should be examined before any further results are addressed. Fig. 15 shows a plot of the dimensionless wind velocity profile, $\phi_m$,

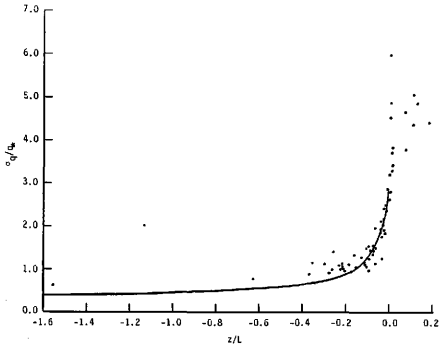


Fig. 11. Normalized standard deviations of humidity fluctuations for 30-min averaging times at the 15.2 m tower level versus stability. The curve denotes $\sigma_q/q_* = b(-z/L)^{-1/3}$ with b = 0.50.

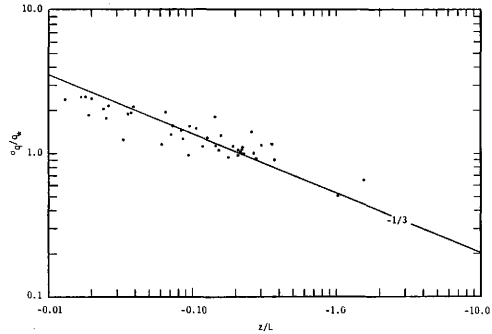


Fig. 12. Normalized standard deviations of humidity fluctuations versus stability, as in Fig. 11, in a log-log plot. The solid line indicates the -1/3 slope expected from theory.

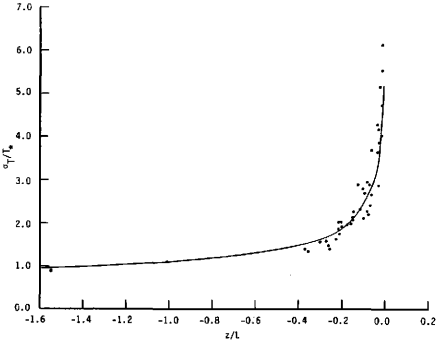


Fig. 13. Normalized standard deviations of temperature fluctuations for 30-min averaging times at the 15.2 m tower level versus stability. The curve denotes $\sigma_T/T_* = b(-z/L)^{-1/3}$ with b = 1.10.

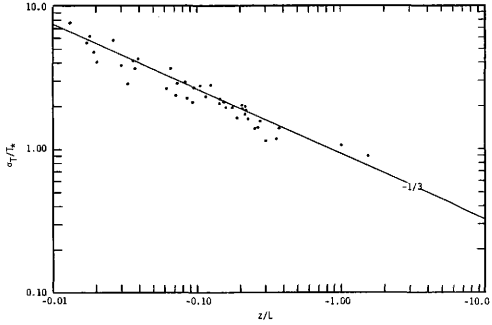


Fig. 14. Normalized standard deviations of temperature fluctuations versus stability, as in Fig. 13, in a log-log plot. The solid line indicates the -1/3 slope expected from theory.

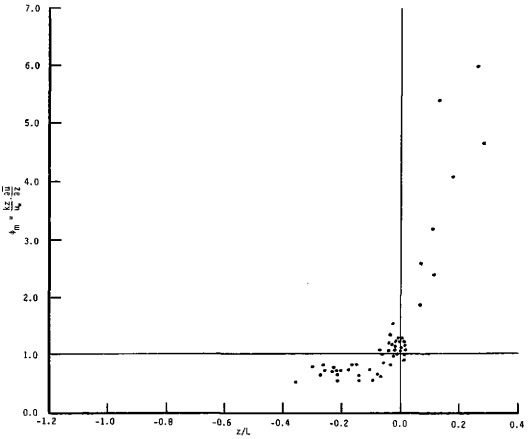


Fig. 15. Nondimensional velocity profile, $\phi_m$, versus stability.

against stability. $\phi_m$ is defined as

$$\phi_m (z/L) = \frac{kz}{u_*} \frac{\partial \bar{u}}{\partial z} \quad , \tag{6.2}$$

where k is the von Karman constant. In order to reproduce a log wind profile in the surface layer, $\phi_m$ must be equal to one at neutral stability. However, it can be seen from Fig. 15 that the value at neutral stability is approximately 1.15. Thus in order to have a log layer, the value of the von Karman constant must be 0.35 instead of the more commonly used value of 0.40. This value of k = 0.35 is in agreement

with the results of Businger et al. (1971) who arrived at the same value in an analysis of the Kansas data. Therefore in this study, a value of $k = 0.35$ was used in all of the calculations.

b. Humidity variance budget

Referring to Chapter 4, two different forms of the humidity variance budget equation, (4.9) and (4.10), were derived. The differences between these equations were in the forms of the production term (the second term in each equation) and the term R*, which arise from the fact that two different averaging times were used. These differing terms will be examined here to see whether the results obtained from the two equations are significantly different.

If one assumes that the turbulence properties are stationary with respect to time, then

$$\frac{1}{2}\frac{\partial\overline{(q')^2}}{\partial t} = 0 \tag{6.3}$$

is a good approximation for the first term in the two equations. Calculations of this term using the data show this term to be quite small for all runs, and therefore this term may be dropped from both equations. In addition, the term

$$R^* = \left(\overline{q'\frac{\partial\hat{q}}{\partial t}} + \overline{q'\frac{\partial\hat{w}\hat{q}}{\partial z}}\right) \tag{6.4}$$

from (4.9) was calculated for each run and found to be at least 2 orders of magnitude smaller than the largest component of the budget in almost

all cases. Therefore this term was also assumed to be negligible. Lastly, the two different forms of the production term

$$\text{Prod 1} = \overline{w'q' \frac{\partial \hat{q}}{\partial z}} ,$$

and

$$\text{Prod 2} = \overline{w'q'} \frac{\partial \bar{q}}{\partial z} \tag{6.5}$$

were calculated and plotted against each other to see if they were of similar magnitude over the whole range of stability (Fig. 16). The

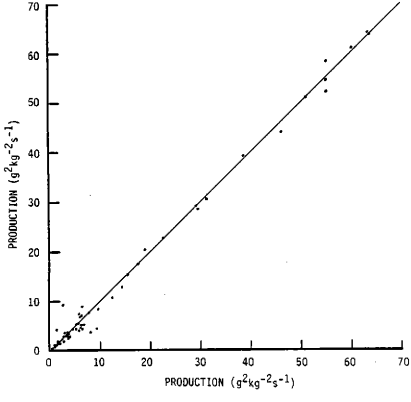


Fig. 16. Production term in (4.9) plotted against the production term in (4.10). The solid line indicates a 1:1 relationship.

values group very close to the line denoting a perfect correlation, indicating that the differences between the two terms are very small. So taking into account all of these results, one can conclude that the two different forms of the variance budget equation yield similar results, and either form can be used. For simplicity in making comparisons with other studies, the more traditional form of the equation, (4.10), will be the one analyzed more closely.

*In* evaluating the remaining terms in (4.10), one problem was encountered. Apparently some of the humidity and temperature sensors were not properly calibrated, leading to errors in the measurement of the mean vertical gradients. Since the production term was computed using these gradients, it is most likely larger or smaller by some constant value than computed. Since this error was most likely constant over the whole time period in which the data were collected, the shape of the curves derived will not be affected. Therefore, in order to compare the variation of the production term with stability against the variations of the other terms, the production term was normalized by the value at neutral stability. This nondimensional, normalized production term is plotted against the stability parameter, z/L in Fig. 17. There appears to be a strong functional relationship with stability for this production term.

Fig. 18 shows the third term in (4.10), the turbulent transport, plotted against stability. There is no observable relationship with stability present in this graph, and the computed values were quite small in comparison to the production term. A few large values can be seen near neutral stability, but these are probably anomolies due to the

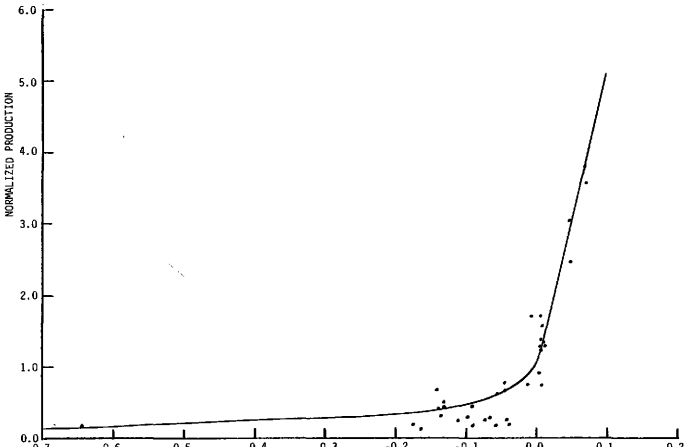


Fig. 17. Normalized nondimensional production of humidity variance versus stability.

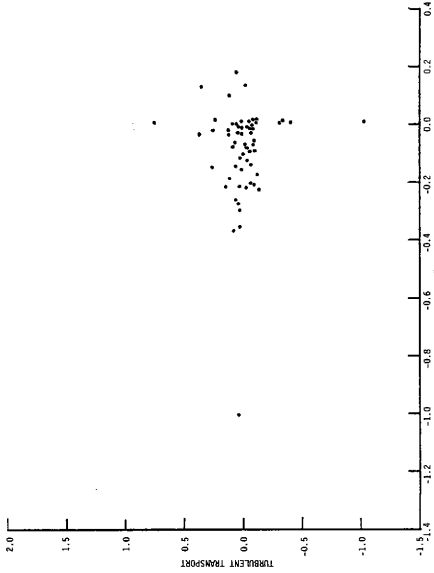


Fig. 18. Nondimensional turbulent transport of humidity variance versus stability.

strange behavior of the scaling parameters at neutral stability. Therefore, it is assumed that this term does not significantly contribute to the variance budget and can be neglected. In addition, the term R which denotes the horizontal gradients and source/sink terms, none of which were measured, is assumed to be zero since the turbulence appears to be horizontally homogeneous and lacking in significant sources and sinks. The omission of these terms leaves only the dissipation term to be examined. Fig. 19 is a plot of the normalized dissipation of the humidity variance, computed from the structure function parameters. It shows also a strong functional relationship with stability.

If one compares the curves from Fig. 17 and Fig. 19, as done in Fig. 20, it can be seen that the production and dissipation terms exhibit almost identical functional relationships with stability. Since these are the only two significant terms left in the equation, and they exhibit this similar relationship with stability, one can safely assume that the production and dissipation of humidity variance are in balance. This is the same result arrived at by Champagne et al. (1977), but is based on more observations and more rigorous calculations than their study. This also is the same result that Wyngaard and Cote´ (1971) arrived at for the temperature variance budget.

Next, the results from the humidity variance budget can be compared with the results of a similar budget performed for temperature variance. This temperature variance budget also showed production and dissipation to be in balance, and Fig. 21 shows the production terms for both humidity and temperature superimposed on one another. It can be seen that they have nearly the same form over the whole stability range.

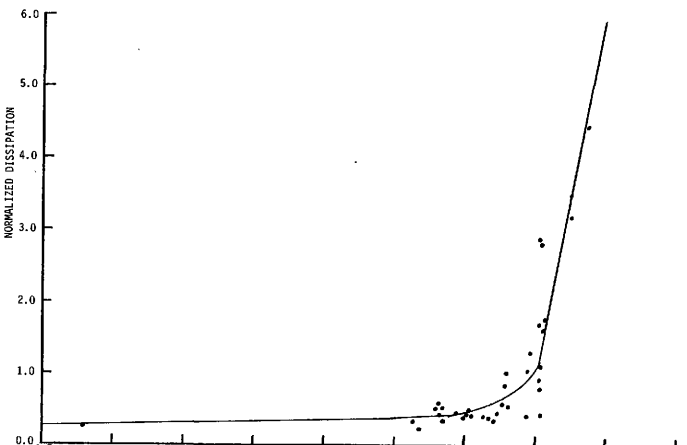


Fig. 19. Normalized nondimensional dissipation of humidity variance versus stability.

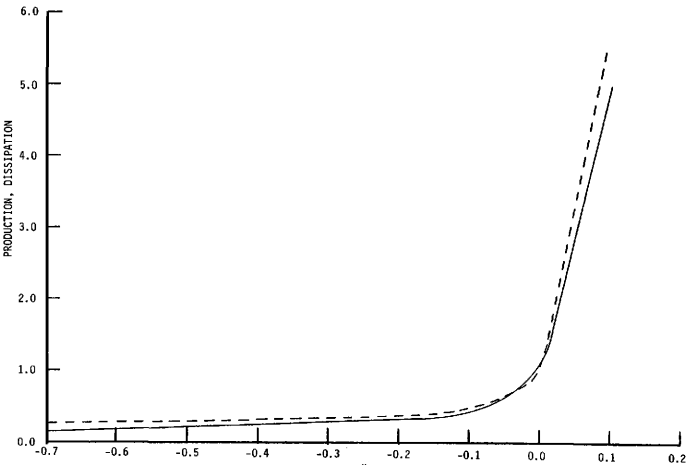


Fig. 20. Comparison of production and dissipation of humidity variance curves. The solid curve is production and the dashed curve is dissipation.

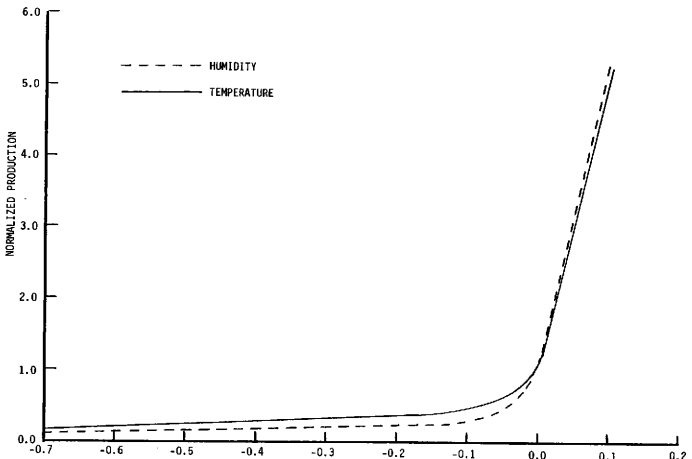


Fig. 21. Comparison of production of humidity variance and production of temperature variance curves.

However, the two curves could differ by a constant value, since their magnitudes are in question due to the mean vertical gradient problem. Therefore, it can be concluded that the budgets of humidity and temperature variance behave similarly, but individual components may differ by a constant value.

The shapes of the production versus stability curves for temperature and humidity computed here do not agree closely with those of other investigators. Fig. 22 shows the production of temperature variance curve against stability from this study compared with the one derived by Wyngaard and Cote´ (1971). They have the same general shape, but have different slopes as one moves away from neutral stability in either direction. These differences are likely due to some bias present in the scaling parameters, $q_*$ and $T_*$. Both $q_*$ and $T_*$ are smaller in the stable region, and larger in the unstable region than the values found by other investigators using similar data. These differences cause the differences in the slopes of the curves found in this study and those of other investigators. The cause of the bias is difficult to determine, but could easily be due to differences in the filtering technique or averaging times. It is important to note that this bias only causes difficulty in comparing the results in this study with those of previous studies, and does not affect any comparisons between the temperature and humidity relationships found in this study alone.

c. Flux-profile relationships

Dimensionless humidity and temperature gradients, $\phi_T$ and $\phi_q$, were computed using the production term in the variance budget equations.

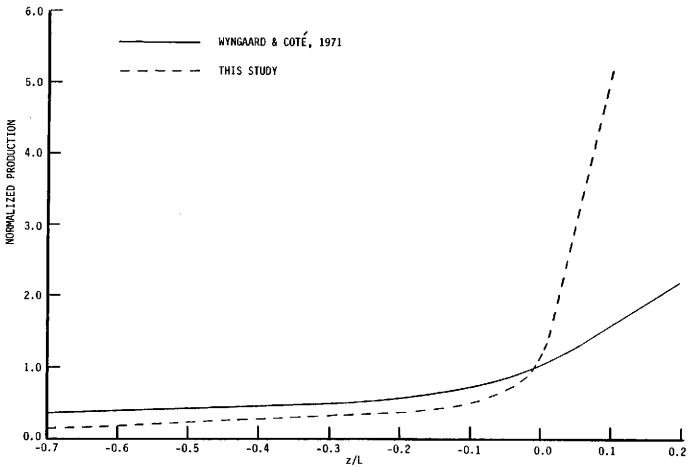


Fig. 22. Normalized nondimensional production of humidity variance curve compared with that of Wyngaard and Cote´ (1971).

These gradients were normalized using the value at neutral stability for comparison purposes, due to the uncertainty of the measured mean vertical gradients. Fig. 23 shows the normalized values of and plotted against z/L. Both terms show the same functional relationship with stability, but could differ by a constant value. Therefore, the assumption that humidity and temperature flux-profile relationships have the same form is a good one, but more accurate measurements of the mean vertical gradients are required to determine whether the relationships are identical.

Fig. 24 shows the experimental values from this study along with the relationship of Businger et al. (1971) who found

$$\phi_T \approx \phi_q = 0.74\ [1-9(z/L)]^{-1/2}\ ,\ \text{for } z/L \leq 0\ ,$$

and

$$\phi_T = \phi_q = 0.74\ [1+4.7(z/L)]\ ,\ \text{for } z/L > 0\ , \qquad (6.6)$$

and that of Dyer and Hicks (1970) who found for the unstable range

$$\phi_q = [1-16(z/L)]^{-1/2}\ , \qquad (6.7)$$

coupled with the equation found by Webb (1970) for the stable range

$$\phi_q = 1 + 5.2\ (z/L)\ . \qquad (6.8)$$

All of these curves were normalized by their values at neutral stability for comparison purposes. The shapes of the curves on the unstable side are quite similar, but the values calculated in this study are consistently lower than those from the earlier studies. In the stable region,

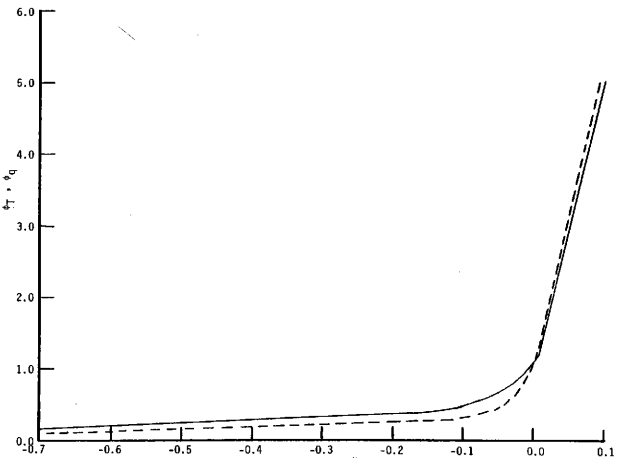


Fig. 23. Normalized nondimensional temperature and humidity profiles, $\phi_T$ and $\phi_q$, versus stability. The solid line is humidity and the dashed curve is temperature.

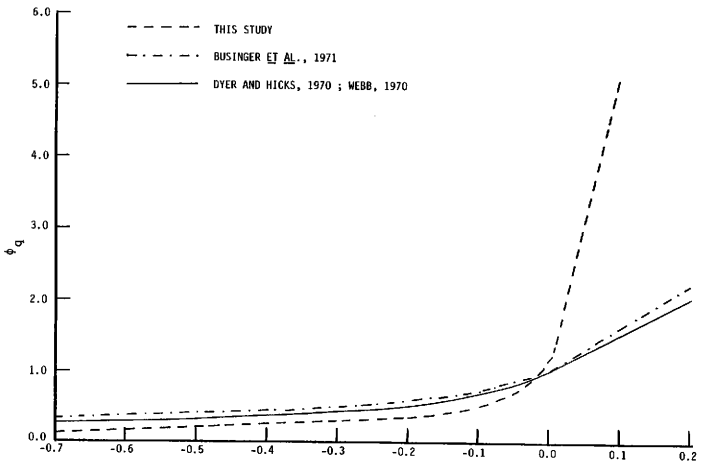


Fig. 24. Normalized nondimensional humidity profile compared with those of other investigators.

the slope of the curve predicted by the data in this study is much greater than that of the other studies. These differences can likely be attributed to the bias apparent in the scaling parameters $q_*$ and $T_*$.

d. Spectra

Spectra of the turbulent fluctuations of humidity, temperature, and the downstream component of the wind were computed for ten of the 2-hour runs. These runs, summarized in Table 6, were chosen to give a representative sample of the whole data set. The purpose for examining these spectra was to see if they were in agreement with the expectations of theory and previous results, and to serve as a further check on the quality of the data. In addition, these spectra were required for the computation of the function parameters and for the estimation of the dissipation rates.

Table 6. Runs for which spectra were computed for the lowest tower level.

| Run # | Run # |
|---|---|
| 6A-B | 14A-D |
| 9A-D | 15A-D |
| 10A-D | 16A-D |
| 12A-D | 17A-D |
| 13A-D | 20A-D |

Figs. 25 and 26 are examples of the normalized spectrum of humidity fluctuations for an unstable case and a stable case, respectively, plotted in logarithmic coordinates. The abscissa is the nondimensional frequency, f, defined by

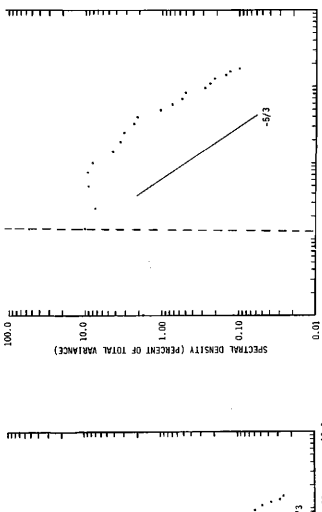


Fig. 25. Normalized spectrum of humidity fluctuations for run #14A, z/L = - 0.139. The solid line denotes the -5/3 slope expected from theory, and the dashed line indicates the low frequency cutoff of the filter.




Fig. 26. Normalized spectrum of humidity fluctuations as in Fig. 25 for run #17A, z/L = 0.049.

$$f = \frac{nz}{U} \tag{6.9}$$

where n is the frequency (in cycles per second), U is the mean wind speed, and z is the height above the ground (the 9.7 m tower level was used in this example). The vertical line in each of the figures indicates the low frequency cutoff of the filter used, with almost all of the lower frequencies having been filtered out of the data. Both curves show the -5/3 slope predicted by Kolmogorov theory for the inertial subrange, with this slope extending over the frequency range of $f = 0.1$ to $f = 1.0$. This result is in good agreement with the findings of Smedman-Högström (1972), who also found a -5/3 slope in this region of the spectrum for humidity. Therefore, these results confirm the existence of an inertial subrange in the spectrum of humidity fluctuations. The spectra for temperature and the downstream component of the wind also took the form of the relationships predicted by theory, indicating that the quality of the turbulence data is good.

Fig. 27 shows the high frequency end of the humidity spectrum for the unstable example given above. The curved line in this figure corresponds to the -5/3 slope in the logarithmic representation of Fig. 25. The data appear to deviate from this curve for $f \geq 1.2$, which is a result of the fact that this is quite close to the high frequency limit of the instruments used in gathering the data, and therefore the spectral energy is decreasing due to the fact that the instruments were unable to measure perfectly these high frequency oscillations.

In computing the spectra, the autocorrelation functions of the humidity, temperature, and wind data themselves were examined. This

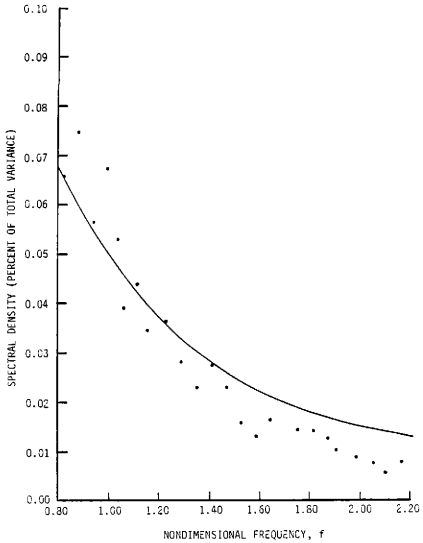


Fig. 27. Normalized spectrum of humidity fluctuations for run #14A, z/L = - 0.139, in a linear representation. The curve indicates a -5/3 relationship with frequency.

examination revealed that for long lags, there was a consistent negative autocorrelation. This indicated that the data probably had been filtered too much, and that too many of the low frequency oscillations were included in the perturbation components of the variables. A test run was made using a filter with a higher cutoff frequency to see if there

would be significant differences in the results from the data using different filters. No significant differences were found in any of the turbulence quantities computed between the two data sets, indicating that the excessive filtering did not affect the final results significantly.

e. Structure function parameters and humidity flux estimates

Humidity structure function parameters were computed for several runs using (5.7) in the spectral range from f = 0.1 to f = 1.0. The runs selected are those listed in Table 6. Fig. 28 is a plot of the nondimensional humidity structure parameter against stability, and it is clear that a functional relationship with stability is present. The solid line in Fig. 28 is the relationship found by Fairall et al. (1980) for the humidity structure function parameter as a function of stability, using data collected over the ocean. They found that this relationship, $C_q^2 = f(z/L)$, could be represented by

$$f(z/L) = 4.0\,[1-7(z/L)]^{-2/3} \quad \text{for } z/L \leq 0 \ ,$$

and

$$f(z/L) = 4.0\,[1+2.4(z/L)]^{2/3} \quad \text{for } z/L > 0 \ . \qquad (6.10)$$

This is the same relationship that Wyngaard et al. (1971a) found for the temperature structure function parameter, $C_T^2 = g(z/L)$, with the difference of only a constant:

$$g(z/L) = 4.9\,[1-7(z/L)]^{-2/3} \quad \text{for } z/L \leq 0 \ ,$$

and

$$g(z/L) = 4.9\,[1+2.4(z/L)]^{2/3} \quad \text{for } z/L > 0 \ . \qquad (6.11)$$

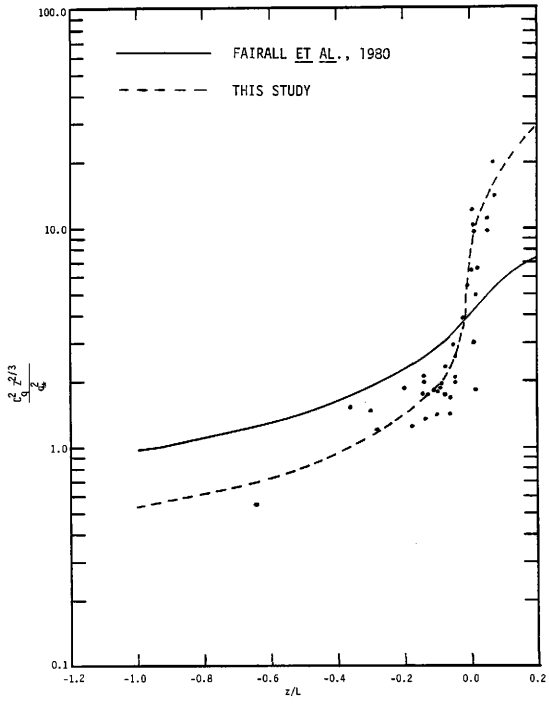


Fig. 28. Nondimensional humidity structure function parameter versus stability.

The humidity structure function parameters calculated from the spectra here do not agree well with these earlier results. There is good agreement on the value at neutral stability, but the data indicate that the nondimensional structure function parameters are higher in the stable range and lower in the unstable range than predicted by the earlier results. Once again this difference may result from the bias in the scaling parameters.

As indicated by (6.9), Fairall et al. (1980) found that the humidity and temperature structure function parameters have the same functional relationship with stability, with the difference of only a constant. To test this finding with the data in this study, the temperature structure function parameters were computed for the same runs listed in Table 6, and plotted against stability (Fig. 29), and curves were fit to these data using the functional forms of Wyngaard et al. (1971a). The humidity structure function parameter (Fig. 28) was found to be fit well by

$$f(z/L) = 4.1\ [1-20(z/L)]^{-2/3} \text{ for } z/L \leq 0 ,$$

and

$$f(z/L) = 4.1\ [1+17(z/L)]^{2/3} \text{ for } z/L > 0 . \qquad (6.12)$$

Fig. 29 shows an approximation for the temperature structure function parameter, $g(z/L)$, which differs from that of humidity by only a constant:

$$g(z/L) = 2.1\ [1-20(z/L)]^{-2/3} \text{ for } z/L \leq 0 ,$$

and

$$g(z/L) = 2.1\ [1+17(z/L)]^{2/3} \text{ for } z/L > 0 . \qquad (6.13)$$

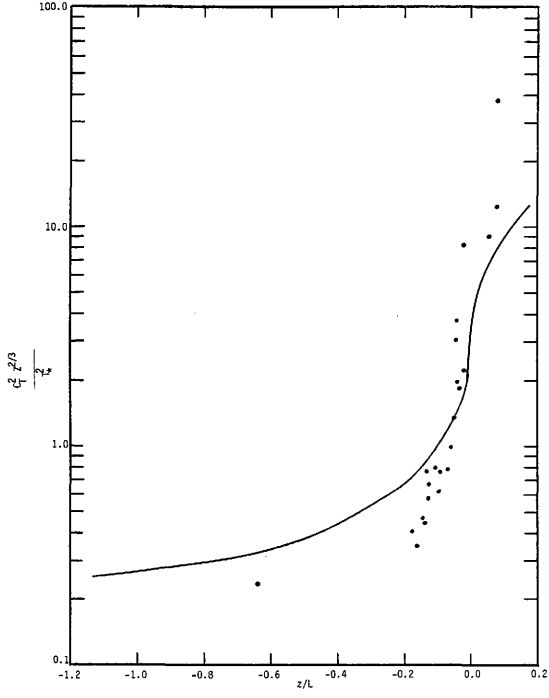


Fig. 29. Nondimensional temperature structure function parameter versus stability.

While this approximation does not fit the data perfectly, it is apparent that the forms of the curves for both temperature and humidity are close enough to be assumed to be the same, given the amount of data points present. However, additional investigations are needed to prove this assumption conclusively.

Wyngaard and Clifford (1978) developed a technique for estimating the fluxes of scalar properties using the values of the structure function parameters. They reasoned that this technique could prove to be useful for flux estimation since the only measurements required are the mean gradients of the wind and scalar properties, and the structure function parameters which can be measured using an optical sensor. They tested this method for heat flux using field data, and found the technique to be only roughly accurate. Since the data collected in this study were applicable to this technique, an evaluation of the technique was made for the estimation of humidity flux.

Wyngaard and Clifford found that the covariance, $M_o = \overline{-q' w'}$, where $M_o$ is proportional to the humidity flux, can be related to the structure function parameters of wind ($C_V^2$) and humidity ($C_q^2$) by

$$M_o = 0.25\ k^{2/3}\ \alpha^{-1/2}\ \beta_q^{2/3}\ (C_V^2)(C_q^2)^{1/2}\ \chi_q^{-1/2}\phi_\varepsilon^{-1/6} \qquad (6.14)$$

where k is the von Karman constant, $\alpha$ and $\beta_q$ are the spectral constants for wind and humidity, and $\chi_q$ and $\phi_\varepsilon$ are the nondimensional dissipation rates of the humidity variance and turbulent kinetic energy. They used the following approximations for the dissipation rates, which were found by experiment:

$$\phi_\varepsilon = \left[1+0.5(z/L)^{2/3}\right]^{3/2} \quad \text{for } z/L \leq 0 \ ,$$

$$\phi_\varepsilon = [1+3.7(z/L)] \quad \text{for } z/L > 0 \ ,$$

$$\chi_q = \frac{2.25}{\left[1-9(z/L)^{1/2}\right]} \quad \text{for } z/L \leq 0 \ ,$$

and

$$\chi_q = 2\,[1.12+4.7(z/L)] \quad \text{for } z/L > 0 \ . \tag{6.15}$$

In the evaluation performed in this study, the values used for the constants were $k = 0.35$, $\alpha = 0.5$, and $\beta_q = 0.6$.

The results of this technique for humidity flux appear in Table 7, along with the humidity flux computed directly from the data using the eddy correlations. Table 8 lists the ratios of the measured fluxes to the structure function parameter derived fluxes. It is clear that this flux estimation technique underestimates the humidity flux in the unstable range, and overestimates the flux in the stable range. These errors are most likely due to the uncertainty in the values of the constants used, and the validity of the approximations used for the dissipation rates, $\chi_q$ and $\phi_\varepsilon$, for this particular site. However, these differences may also be due to the bias apparent in the measurements of the scaling parameters $q_*$ and $T_*$. It is possible to add two different experimental constants to the scheme for the unstable and stable ranges to make the estimates more correct, but there would still be a somewhat large degree of uncertainty in the estimates as evidenced by the large standard deviations of the estimates listed in Table 8. However, the estimates still could be useful if no other method for measuring the fluxes is available.

Table 7. Measured and derived values of the humidity flux.

| Run # | z/L | $M_o$ (measured) g $kg^{-1}$ $ms^{-1}$ | $M_o$ (derived) g $kg^{-1}$ $ms^{-1}$ |
|---|---|---|---|
| 6A | -0.042 | 0.0318 | 0.0280 |
| 6B | -0.167 | 0.0986 | 0.0411 |
| 9A | 0.011 | 0.0039 | 0.0045 |
| 9B | 0.008 | 0.0042 | 0.0057 |
| 9C | 0.006 | 0.0027 | 0.0047 |
| 9D | 0.003 | 0.0074 | 0.0087 |
| 10A | 0.010 | 0.0055 | 0.0057 |
| 10B | 0.007 | 0.0073 | 0.0015 |
| 10C | 0.006 | 0.0063 | 0.0048 |
| 10D | 0.008 | 0.0064 | 0.0050 |
| 12A | -0.021 | 0.0176 | 0.0092 |
| 12B | -0.039 | 0.0177 | 0.0093 |
| 12C | -0.060 | 0.0271 | 0.0111 |
| 12D | -0.012 | 0.0235 | 0.0113 |
| 13A | -0.174 | 0.0369 | 0.0193 |
| 13B | -0.074 | 0.0483 | 0.0232 |
| 13C | -0.137 | 0.0485 | 0.0258 |
| 13D | -0.097 | 0.0451 | 0.0258 |
| 14A | -0.139 | 0.0300 | 0.0207 |
| 14B | -0.644 | 0.0377 | 0.0310 |
| 14C | -0.091 | 0.0419 | 0.0209 |
| 14D | -0.132 | 0.0395 | 0.0243 |
| 15A | -0.142 | 0.0279 | 0.0156 |
| 15B | -0.131 | 0.0300 | 0.0160 |
| 15C | -0.054 | 0.0315 | 0.0157 |
| 15D | -0.045 | 0.0220 | 0.0123 |
| 16A | -0.046 | 0.0153 | 0.0109 |
| 16B | -0.023 | 0.0120 | 0.0101 |
| 16C | -0.008 | 0.0095 | 0.0078 |
| 16D | 0.004 | 0.0054 | 0.0028 |
| 17A | 0.049 | 0.0033 | 0.0049 |
| 17B | 0.049 | 0.0037 | 0.0041 |
| 17C | 0.072 | 0.0030 | 0.0035 |
| 17D | 0.070 | 0.0021 | 0.0035 |
| 20A | -0.172 | 0.0058 | 0.0052 |
| 20B | -0.091 | 0.0122 | 0.0088 |
| 20C | -0.101 | 0.0161 | 0.0098 |
| 20D | -0.068 | 0.0214 | 0.0013 |

Table 8. Ratio of measured to derived humidity fluxes for stable and unstable runs.

| Unstable runs | | Stable runs | |
|---|---|---|---|
| z/L | Measured flux/ derived flux | z/L | Measured flux/ derived flux |
| -0.042 | 1.14 | 0.011 | 0.88 |
| -0.167 | 2.40 | 0.008 | 0.73 |
| -0.021 | 1.91 | 0.006 | 0.57 |
| -0.039 | 1.90 | 0.003 | 0.84 |
| -0.060 | 2.44 | 0.06 | 0.96 |
| -0.112 | 2.09 | 0.007 | 0.49 |
| -0.179 | 1.91 | 0.006 | 1.32 |
| -0.074 | 2.08 | 0.008 | 1.28 |
| -0.137 | 1.98 | 0.049 | 0.69 |
| -0.097 | 1.75 | 0.049 | 0.92 |
| -0.140 | 1.45 | 0.071 | 0.86 |
| -0.644 | 1.22 | 0.071 | 0.61 |
| -0.091 | 2.01 | | |
| -0.132 | 1.58 | Average | 0.84 |
| -0.142 | 1.79 | Standard deviation | 0.25 |
| -0.131 | 1.88 | | |
| -0.054 | 2.01 | | |
| -0.045 | 1.79 | | |
| -0.047 | 1.41 | | |
| -0.022 | 1.22 | | |
| -0.008 | 1.19 | | |
| -0.172 | 1.11 | | |
| -0.091 | 1.39 | | |
| -0.101 | 1.64 | | |
| -0.068 | 1.67 | | |
| Average | 1.72 | | |
| Standard deviation | 0.36 | | |

## 7. CONCLUSIONS

It is apparent from this study that the budgets of humidity and temperature variance in the atmospheric surface layer behave similarly. The production and dissipation of the humidity variance are in local balance, which is the same result found for temperature variance. Further, the production versus stability curves for humidity and temperature variance have the same functional form, with perhaps the difference of only a constant. However, these functional forms differ from those found by previous investigators for both the stable and unstable ranges of z/L. It is possible that these differences are due to a bias in the computation of the scaling parameters, $q_*$ and $T_*$.

It was found that the humidity flux-profile relationship has the same functional form as that for temperature, with perhaps the difference of a constant. Again, these functional forms differed from those found by previous investigators, and point to the problem with the turbulence scaling parameters.

The humidity structure function parameters computed from the humidity spectra showed a clear functional dependence on stability. A dependence on stability was also found for the temperature structure function parameter, however it was not clear whether these functional forms were the same. It is probable though that the humidity and temperature structure function parameters have the same functional form, with the difference of a fairly large constant. It was found that it is possible to estimate the humidity flux from the structure function parameters, using the technique of Wyngaard and Clifford (1978), with a fair degree of accuracy. The method underestimated the humidity flux in

the unstable range, and overestimated the flux in the stable range, but the use of an added experimental constant could eliminate these errors.

Lastly, the micrometeorological tower and data acquisition system yielded high quality turbulence data in the spectral range of up to $f \sim 1.5$. The spectra computed as a check on the quality of the data confirmed the existence of the inertial subrange for humidity fluctuations, and all other turbulence quantities calculated followed the relationships expected from theory and the results of previous studies. The high quality of the measurements and the turbulence data give added support to the results presented in this study.

## 8. SUGGESTIONS FOR FURTHER RESEARCH

During the course of this research it became apparent that there are several topics related to this research that bear further study, and could be used to form the basis for future research projects. For instance, a detailed analysis of the fluxes of humidity and sensible heat should be performed to determine if their behavior is similar. Is there a direct correlation between the humidity flux and the heat flux? Are the same size eddies responsible for both fluxes? Do they have the same integral scale?

Another area for research is to study the sensitivity of the kinetic energy budget to differences in averaging times, similar to the analysis performed in this study for the humidity variance budget. Lastly, a field study could be performed using two different sites with markedly different surface conditions to determine if the relationship between the turbulence scaling parameters $q_*$ and $T_*$ and the stability parameter z/L is truly universal, or is it affected by differences between sites.

## REFERENCES


Blackman, R. B., and J. W. Tukey, 1958: The Measurement of Power Spectra. Dover Publications, 190 pp.

Busch, N. E., 1973: On the Mechanics of Atmospheric Turbulence. Workshop on Micrometeorology, Amer. Meteor. Soc., 1-65.

Businger, J. A., J. C. Wyngaard, Y. Izumi, and E. F. Bradley, 1971: Flux-profile relationships in the atmospheric surface layer. J. Atmos. Sci., 28, 181-189.

Champagne, F. H., C. A. Friehe, J. C. LaRoe and J. C. Wyngaard, 1977: Flux measurements, flux estimation techniques, and fine-scale turbulence measurements in the unstable surface layer over land. J. Atmos. Sci., 34, 515-529.

Drinkrow, R., 1972: A solution to the paired Gill-anemometer response function. J. Appl. Met., 11, 76-80.

Dyer, A. J., and B. B. Hicks, 1970: Flux-gradient relationships in the constant flux layer. Quart. J. Roy. Meteor. Soc., 96, 715-721.

Fairall, C. W., G. E. Schacher and K. L. Davidson, 1980: Measurements of the humidity structure function parameters, $C_q^2$ and $C_{T_q}$, over the ocean. Bound.-Layer Meteor., 19, 81-92.

Haugen, D. A., J. C. Kaimal, and E. F. Bradley, 1971: An experimental study of Reynold's stress and heat flux in the atmospheric surface layer. Quart. J. Roy. Meteor. Soc., 97, 161-180.

Horst, T. W., 1973: Corrections for response error in a three-component propellor anemometor. J. Appl. Met., 12, 716-725.

Kaimal, J. C., J. C. Wyngaard, Y. Izumi and O. R. Cote', 1972: Spectral characteristics of surface layer turbulence. Quart. J. Roy. Meteor. Soc., 98, 563-589.

Lumley, J. L., and H. A. Panofsky, 1964: The Structure of Atmospheric Turbulence. John Wiley and Sons, 239 pp.

MacCready, P. B., and H. R. Jex, 1964: Response characteristics and meteorological utilization of propellor and vane wind sensors. J. Appl. Met., 8, 182-193.

Monin, A. S., and A. M. Obukhov, 1953: Dimensionless characteristics of turbulence in the atmospheric surface layer. Doklady AN SSSR, 93, 223-226.

_____, and A. M. Obukhov, 1954: Basic turbulent mixing laws in the atmospheric surface layer. Trudy Geofiz. Inst. AN SSSR, 24, 163-187.

Panofsky, H. A., and G. W. Brier, 1958: Some Applications of Statistics to Meteorology. The Pennsylvania State University, 224 pp.

_____, 1969: The spectrum of temperature. Radio Sci., 4, 1143-1146.

Smedman-Högström, A. S., 1972: Temperature and humidity spectra in the atmospheric surface layer. Bound.-Layer Meteor., 3, 329-347.

Webb, E. K., 1970: Profile relationships: The log-linear range and extension to strong stability. Quart. J. Roy. Meteor. Soc., 96, 67-90.

Wyngaard, J. C., and O. R. Cote´, 1971: The budgets of turbulent kinetic energy and temperature variance in the atmospheric surface layer. J. Atmos. Sci., 27, 190-201.

_____, Y. Izumi, and S. F. Collins, 1971a: Behavior of the refractive index structure parameter near the ground. J. Opt. Soc. Am., 61, 1646-1650.

_____, O. R. Cote´ and Y. Izumi, 1971b: Local free convection, similarity and budgets of shear stress and heat flux. J. Atmos. Sci., 28, 1171-1182.

_____, 1973: On Surface-Layer Turbulence. Workshop on Micrometeorology, Amer. Meteor. Soc., 101-149.

_____, and S. F. Clifford, 1978: Estimating momentum, heat and moisture fluxes from structure parameters. J. Atmos. Sci., 35, 1204-1211.

Yaglom, A. M., 1977: Comments on wind and temperature flux-profile relationships. Bound.-Layer Meteor., 11, 89-102.

# VITA

Scott Richard Humphrey was born August 22, 1961 in Lakewood, Ohio, the third son of Sandra T. and Richard D. Humphrey. He graduated from Conestoga Senior High School in Berwyn, Pennsylvania in 1979, and attended The Pennsylvania State University from 1979-1981. He received his B.S. in meteorology from Texas A&M in May 1983, and accepted a Lechner Fellowship to continue his education at that school. He received his M.S. degree from Texas A&M University in May 1985, with a degree emphasis in the area of atmospheric turbulence.

Mr. Humphrey's permanent address is: 16130 Red Cedar Trail, Dallas, Texas 75248.